Crystal Bonding

Contents

Abstract

The bonding of atoms in semiconductors is accomplished by electrostatic forces – Coulomb forces between the electrons and atomic nuclei – and the tendency of atoms to fill their outer shells. Interatomic attraction is balanced by short-range repulsion due to strong resistance of atoms against interpenetration of core shells. Coulomb forces are the basis for ionic and hydrogen bonding forces but are also involved in metallic bonding and, as dipole–dipole interaction, in van der Waals bonding. In addition, strong quantum-mechanical effects, determining specific orbitals, and Pauli exclusion are major contributing factors in covalent and metallic bonding, respectively.

1 Ionic and Covalent Bonding

Interatomic Forces In this chapter, the different types of bonding of solids are reviewed, irrespective of whether the solids are crystalline or amorphous. This treatment is quite general and is not restricted to semiconductors.

The formation of solids is determined by the interatomic forces and the size of the atoms shaping the crystal lattice. The interatomic forces are composed of a far-reaching attractive and a short-range repulsive component, resulting in an *equilibrium distance* of vanishing forces at an interatomic distance r_e, at which the potential energy shows a minimum (Fig. 1). In binary compounds, this equilibrium distance, r_e, can be written as the sum of *atomic radii*,

$$r_e = r_A + r_B, \tag{1}$$

where r_A and r_B are characteristic for the two atoms A and B (Fig. 2) and can be used when other binary compounds are formed with the same bonding type, containing A or B. For a more detailed discussion on atomic radii, see Sect. 3.1.

Attractive interatomic forces are predominantly electrostatic in character (e.g., in ionic, metallic, van der Waals, and hydrogen bonding) or are a consequence of sharing valence electrons of atoms to fill their outer shells, resulting in covalent bonding. Most materials show mixed bonding, i.e., at least two of these bond types contribute significantly to the interatomic interaction. In most technologically important compound semiconductors, these mixed bondings are more covalent and less ionic. In

Fig. 1 Interaction potential eV between two atoms; r_e is the equilibrium distance; E_b is the bonding energy at $r = r_e$
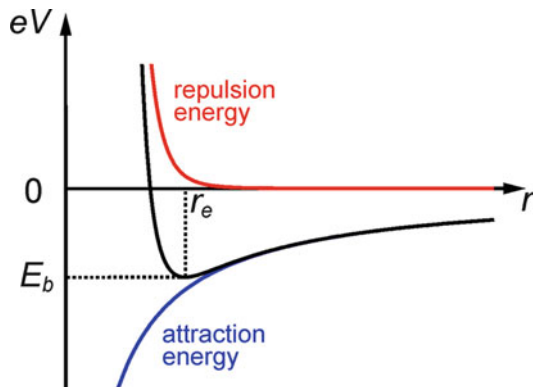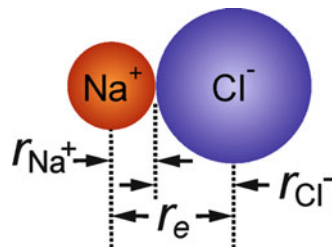

Fig. 2 Na^+ anion and Cl^- cation shown as hard spheres in actual ratio of radii

other semiconductors, one of the other types may contribute, e.g., van der Waals bonding in organic crystals and metallic bonding in highly conductive semiconductors. These different bonding types will be discussed in the following sections.

The *repulsive interatomic forces*, called Born forces (see Born and Huang 1954), are caused by a strong resistance of the electronic shells of atoms against interpenetration. The repulsive Born potential is usually modeled with a strong power law[1]

$$eV(r) = \beta/r^m, \quad m \approx 10 \ldots 12, \tag{3}$$

with β the force constant (see Eq. 1 in chapter ▸ "Elasticity and Phonons") and m an empirical exponent (see Sect. 1.1). For ionic crystals, the exponent m is somewhat smaller ($6 < m < 10$).

1.1 Ionic Bonding

Ionic bonding is caused by Coulomb attraction between ions. Such ions are formed by the tendency of atoms to complete their outer shells. This is most easily accomplished by compounds between elements of group I and group VII of the periodic system of elements; here, only one electron needs to be exchanged. For instance, in a NaCl crystal, the Cl atom captures one electron to form a negative Cl^- ion and the Na atom loses the single electron in its outer shell to become a positive Na^+ ion. The bonding is then described by isotropic (radial-symmetric) *nonsaturable* Coulomb forces attracting as many Na^+ ions as space permits around each Cl^- ion, and vice versa, while maintaining overall neutrality, i.e., an equal number of positive and negative ions. This results in a closely packed NaCl lattice with a coordination number 6 (=number of nearest neighbors).

The energy gain between two ions can be calculated from the potential equation

$$eV = -\frac{e^2}{4\pi\varepsilon_0 \; r} + \frac{\beta}{r^m} \quad \text{for } r = r_e, \tag{4}$$

containing Coulomb attraction (first term) and Born repulsion (second term). For an equilibrium distance $r_e = r_{Na^+} + r_{Cl^-} = 2.8\text{Å}$, a minimum of the potential energy of $eV_{\min} \approx -5$ eV results[2] for a typical value of $m = 9$. In a crystal, we must consider *all*

---

[1]A better fit for the Born repulsion is obtained by the sum of a power and an exponential law:

$$V_{\text{Born}} = \beta/r^m + \gamma \exp(-r/r_0), \tag{2}$$

where r_0 is the softness parameter, listed for ions in Table 8. For more sophisticated repulsion potentials, see Shanker and Kumar (1987).

[2]β can be eliminated from the minimum condition ($dV/dr|_{r_e} = 0$). One obtains $\beta = e^2 r_e^{m-1}/(4\pi\varepsilon_0 m)$ and as *cohesive energy* $eV_{\min} = -e^2(m-1)/(4\pi\varepsilon_0 m \; r_e)$.

neighbors. For example, in a NaCl lattice, six nearest neighbors exert Coulomb attraction in addition to 12 next-nearest neighbors of equal charge exerting Coulomb repulsion, etc. This alternating interaction results in a summation that can be expressed by a proportionality factor in the Coulomb term of Eq. 4, the *Madelung constant* (Madelung 1918). For a NaCl crystal structure, we have

$$A = \frac{6}{\sqrt{1}} - \frac{12}{\sqrt{2}} + \frac{8}{\sqrt{3}} - \frac{6}{\sqrt{4}} + \frac{25}{\sqrt{5}} - + \cdots, \tag{5}$$

where each term presents the number of equidistant neighbors in the numerator and the corresponding distance (in lattice units) in the denominator. This series is only slowly converging. Ewald's method (the theta-function method) is powerful and facilitates the numerical evaluation of A. For NaCl, we obtain from (Madelung 1918; Born and Landé 1918)

$$eV = -A\frac{e^2}{4\pi\varepsilon_0} + \frac{\beta'}{r_e^m} \tag{6}$$

with $A = 1.7476$, a lattice binding energy of $eV_{\min}{}^{(A)} = H^0(\text{NaCl}) = 7.948$ eV, compared to an experimental value of 7.934 eV. Here, β' and m are empirically obtained from the observed lattice constant and compressibility. The Madelung constant is listed for several AB compounds in Table 1 (see Sherman 1932).

The Born–Haber cyclic process is an empirical way of obtaining the lattice energy, i.e., the binding energy per mole. The process starts with the solid metal and gaseous halogen and adds the heat of sublimation $W_{\text{subl}}(\text{Na})$ and the dissociation energy $(1/2)W_{\text{diss}}(\text{Cl}_2)$; it further adds the ionization energy $W_{\text{ion}}(\text{Na})$ and the electron affinity $W_{\text{el aff}}(\text{Cl})$ in order to obtain a diluted gas of Na^+ and Cl^- ions; all of these energies can be obtained experimentally. These ions can be brought together from infinity to form the NaCl crystal by gaining the unknown lattice energy $H^0(\text{NaCl})$. This entire sum of processes must equal the heat of formation $W^0(\text{NaCl})$ which can be determined experimentally (Born 1919; Haber 1919):

$$W^0_{\text{solid}} = \left\{ W_{\text{subl}}(\text{Na}) + W_{\text{ion}}(\text{Na}) + \frac{1}{2}W_{\text{diss}}(\text{Cl}_2) + W_{\text{el aff}}(\text{Cl}_2) \right\} + H^0(\text{NaCl}). \tag{7}$$

In this equation, a minor correction of an isothermal compression of NaCl from

Table 1 Madelung constant for a number of crystal structures

Crystal structure	Madelung constant
NaCl	1.7476
CsCl	1.7627
Zincblende	1.6381
Wurtzite	1.6410
CaF_2	5.0388
Cu_2O	4.1155
TiO_2 (rutile)	4.8160

Table 2 Lattice constants a (in Å) and ratio of lattice constants c/a for simple AB compounds (After Weißmantel and Hamann 1979) (for explanation of the different crystal structures, see chapter ▶ "The Structure of Semiconductors")

NaCl structure				CsCl structure		Zinc blende		Wurtzite		
	a		a		a		a		a	c/a
AgF	4.93	NaBr	5.973	BaS	6.363	AlP	5.431	AgI	4.589	1.63
AgCl	5.547	NaI	6.433	CsCl	4.118	AlAs	5.631	AlN	3.110	1.60
AgBr	5.775	PbS	5.935	CsBr	4.296	AlSb	6.142	BeO	2.700	1.63
BaO	5.534	PbSe	6.152	CsI	4.571	BeS	4.86	CdS	4.139	1.62
BaS	6.363	PbTe	6.353	TiI	4.206	BeSe	5.08	CdSe	4.309	1.63
BaSe	6.633	RbF	5.651	TlCl	3.842	BeTe	5.551	GaN	3.186	1.62
BaTe	7.000	RbCl	6.553	TlBr	3.978	CSi	4.357	InN	3.540	1.61
CaO	4.807	RbBr	6.868	TiI	4.198	CdS	5.832	MgTe	4.529	1.62
CaS	5.690	RbI	7.341	NH_4Cl	3.874	CdSe	6.052	MnS	3.984	1.62
CaSe	5.992	SnAs	5.692	NH_4Br	4.055	CdTe	6.423	MnSe	4.128	1.63
CaTe	6.358	SnTe	6.298	NH_4I	4.379	CuF	4.264	TaN	3.056	–
CdO	4.698	SrO	5.156	$TlNO_3$	4.31	CuCl	5.417	ZnO	3.249	1.60
KF	5.351	SrS	5.582	CsCN	4.25	CuBr	5.691	ZnS	3.819	1.64
KCl	6.283	SrSe	6.022			GaP	5.447	NH_4F	4.399	1.60
KBr	6.599	SrTc	6.483			GaAs	5.646			
KI	7.066	TaC	4.454			GaSb	6.130			
LiF	4.025	TiC	4.329			HgSe	6.082			
LiCl	5.130	TiN	4.244			HgTe	6.373			
LiBr	5.501	TiO	4.244			InAs	6.048			
LiI	6.012	VC	4.158			InSb	6.474			
MgO	4.211	VN	4.137			MnS	5.611			
MgS	5.200	VO	4.108			MnSe	5.832			
MgSe	5.462	ZrC	4.696			ZnS	5.423			
NaF	4.629	ZrN	4.619			ZnSe	5.661			
NaCl	5.693					ZnTe	6.082			

$p = 0$ to $p = 1$ atm, heating from $T = 0$ K to room temperature, and an adiabatic expansion of the ion gases to $p = 0$ have been neglected. The corresponding energies almost cancel. The error is $<1\%$.

A listing of lattice constants (for definition, see chapter ▶ "The Structure of Semiconductors") of a number of predominantly ionic AB compounds is given in Table 2.

1.2 Covalent Bonding

Covalent bonding is caused by two electrons that are shared between two atoms: they form an electron bridge. The bridge formation can be understood quantum-mechanically by a nonspherical electron-density distribution that extends between the bonded atoms. Examples of such density distributions are shown schematically
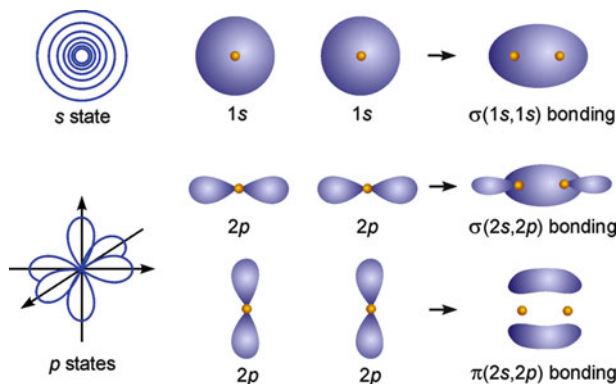
Fig. 3 Atomic and molecular electron-density distribution for $\sigma(s)$, $\sigma(p)$, and $\pi(p)$ bonding (After Weißmantel and Hamann 1979)
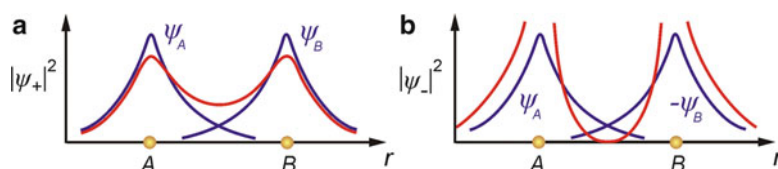

Fig. 4 Wave functions of one-electron states [*blue curves* – identical in (**a**) and (**b**)] and probability function to find one electron (*red curves*) in (**a**), a bonding state, and (**b**), an antibonding state, showing finite and vanishing electron density at the center between atoms A and B for these two states, respectively [observe the plotting of $-\psi_B$ in (**b**)]. The picture of these two one-electron states shown here shall not be confused with the two-electron potential given in Fig. 5

in Fig. 3 for a molecule formation with electrons in a $1s$ or $2p$ state, e.g., for H_2 or F_2, respectively.

If an atom approaching another atom of the same element has in its protruding part of the electron-density distribution an unpaired electron with antiparallel spin, both eigenfunctions may overlap; the Pauli principle is not violated. Their combined wave function ($\psi_+ = \psi_A + \psi_B$) yields an increased electron density $|\psi_+|^2$ in the overlap region (see Fig. 4a); the result is an *attractive force* between these two atoms in the direction of the overlapping eigenfunctions. This is the state of lowest energy of the two atoms, the *bonding state*. There is also a state of higher energy, the *antibonding state*, with $\psi_- = \psi_A - \psi_B$ in which the spin of both electrons is parallel. Here, the electrons are strongly repulsed because of the Pauli principle, and the electron clouds cannot penetrate each other; therefore, the electron density between both atoms vanishes (Fig. 4b). The resulting potential distribution as a function of the interatomic distance between two hydrogen atoms forming an H_2 molecule is given in Fig. 5. In this figure, the ground state (bonding) S and the excited state (antibonding) A are shown. The figure also contains as center curve the classical contribution of two H atoms with a charge density corresponding to free atoms. Such bonding is small compared with the covalent bonding.

Fig. 5 Potential energy for the two valence electrons of two covalently bound hydrogen atoms approaching each other. *Upper curve*, antibonding state; *lower curve*, bonding state; *middle curve*, bonding potential from free atom charge distribution. Charge-density distributions shown in the *inset* are for the two covalent states (After Kittel 1996)
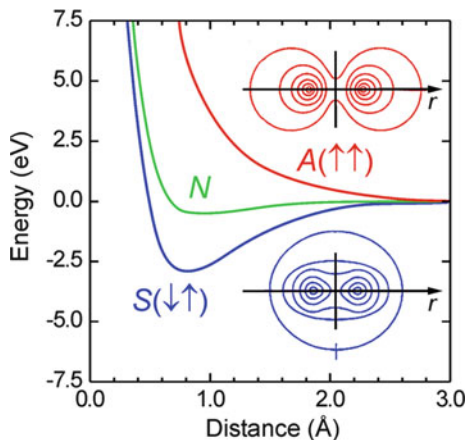
The bond length (center-to-center distance) for some semiconductors and molecules is listed in Table 3. In organic molecules, the bond length between C atoms decreases with increasing bonding valency as shown in the table.

With increasingly missing unpaired electrons in the outer shell, more than one atom of the same kind can be bound to each other. The number of bonded atoms is given by the following valency: monovalent atoms can form only diatomic molecules; divalent atoms, such as S or Se, can form chains; and trivalent atoms, such as As, can form two-dimensional (layered) lattices. Solids are formed from such elements by involving other bonding forces between the molecules, chains, or layers, e.g., van der Waals forces (see Sect. 3). Only tetravalent elements can form three-dimensional lattices which are covalently bound (e.g., Si).

Tetrahedrally Bound Elements Silicon has four electrons in its outer shell. In the ground state of an isolated atom, two of the electrons occupy the *s* state and two of them occupy *p* states, with a $2s^2 2p^2$ configuration. By investing a certain amount of promotion energy,[3] this $s^2 p^2$ configuration is changed into an sp^3 configuration, in which an unpaired electron sits in each one of the four singly occupied orbitals with tetrahedral geometry (see Fig. 6). From the *s* orbital and the three *p* orbitals, four linear combinations can be formed (depending upon the choice of signs), represented as $\sigma_i = 1/2 (\varphi_s + \varphi_{px} + \varphi_{py} + \varphi_{pz})$. This is referred to as *hybridization*, with σ_i as the *hybrid function* responsible for bonding. When we bring together a large number of Si atoms, they arrange themselves such that each of them has four neighbors in tetrahedral geometry as shown in ▶ Fig. 9 of chapter "The Structure of

---

[3]The promotion energy is 4.3, 3.5, and 3.3 eV for C, Si, and α-Sn, respectively. However, when forming bonds by establishing electron bridges to neighboring atoms, a substantially larger energy is gained, therefore resulting in net binding forces. Diamond has the highest cohesive energy in this series, despite the fact that its promotion energy is the largest, because its sp^3-sp^3 C–C bonds are the strongest (see Harrison (1980)).

Table 3 Bond lengths relevant to organic molecules, α-Si, and related semiconductors (After Cotton and Wilkinson 1972)

Bond	Bond length (Å)	Bond	Bond length (Å)
C–C	1.54	Si–Si	2.35
C = C	1.38	Si–H	1.48
C = C	1.42 (graphite)	Ge–Ge	2.45
C ≡ C	1.21	Ge–H	1.55
C–H	1.09 (sp^3)	C–Si	1.87

Fig. 6 Linear combination (hybridization) of a $1s$ function (spherical) with $3p$ functions (**a**) results in four sp^3 functions (**b**) which extend toward the four tetrahedra axes 1–4 and result in strongly directional bonding with a bond angle of 109.47°
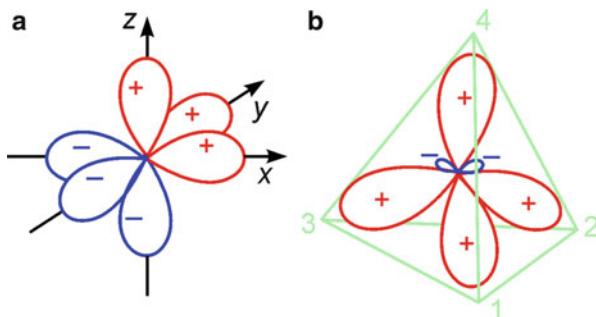
Semiconductors". Each atom then forms four electron bridges to its neighbors, in which each one is occupied with two electrons of opposite spin, as shown for the center atom in Fig. 7a. Such bridges become evident in a density profile within the (110) plane shown for two adjacent unit cells in Fig. 7b.

In contrast to the ionic bond, the covalent bond is angular dependent, since the protruding atomic eigenfunctions extend in well-defined directions. Covalent bonding is therefore a *directional* and *saturable bonding*; the corresponding force is known as a *chemical valence force*, and acts in exactly as many directions as the valency describes.

1.3   Mixed Bonding

Crystals that are bonded partially by ionic and partially by covalent forces are referred to as mixed-bond crystals. Most actual semiconductors have a fraction of covalent and ionic bonding components (see, e.g., Mooser and Pearson 1956).

Tetrahedrally Bonded Binaries By using the Grimm–Sommerfeld rule (see below) for isoelectronic rows of elements, Welker and Weiss (1954) predicted desirable semiconducting properties for III–V compounds.[4] Semiconducting III–V and II–VI compounds are bound in a *mixed bonding*, in which electron bridges exist, i.e., the bonding is directed, but the electron pair forming the bridge sits closer to the

---

[4]Meaning compounds between one element of group III and one element of group V on the periodic system of elements (cf. Fig. 3 in chapter ▶ "Properties and Growth of Semiconductors")
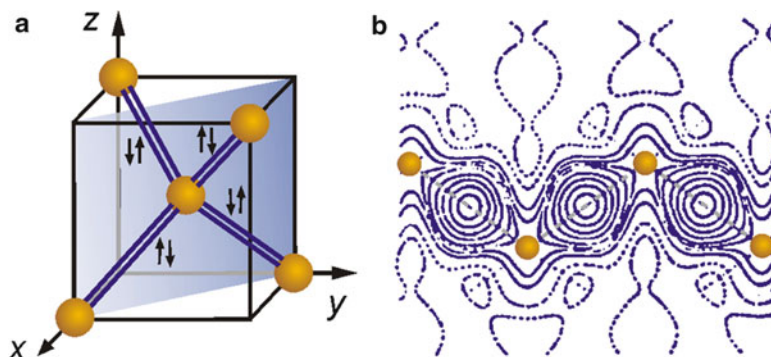
Fig. 7 (**a**) Unit cell of diamond with pairs of electrons indicated between adjacent atoms. (**b**) Electron-density profile within the (110) plane (After Dawson 1967)

anion. This *degree of ionicity* increases for these compounds with an increased difference in electronegativity (Fig. 8) from III–V to I–VII compounds and within one class of compounds, e.g., from RbI to LiF (see also Table 4).

The mixed bonding may be expressed as the sum of the wave functions describing covalent and ionic bonding:

$$\psi = a\psi_{\text{cov}} + b\psi_{\text{ion}}, \tag{8}$$

with the ratio b/a defining the *ionicity* of the bonding. This bonding can also be described as rapidly alternating between that of covalent and ionic. Over an average time period, a fraction of ionicity (b/a) results. The ionicity of the bonding can be described by a static *effective ion charge e**, as opposed to a dynamic effective ion charge (discussed in ▶ Sect. 1.1 in chapter "Photon–Phonon Interaction"), which is less by a fraction on the order of b/a than in a purely ionic compound with the charge given by the valency. For instance, in CdS, the divalent behavior of Cd and S could result in a doubly charged $Cd^{++}S^{--}$ lattice, while measurements of the electric dipole moment indicate an effective charge of 0.49 for CdS. The static effective charge for other II–VI and III–V compounds is given in Table 4.

The effective charge concept can be confusing if one does not clearly identify the ionic state of the system. For instance, in the case of CdS, a purely ionic state is $Cd^{2+}S^{2-}$, as opposed to the covalent state of $Cd^{2-}S^{2+}$ (which is equivalent to the Si^0 Si^0 configuration). In other words, the covalent state is that in which both Cd and S have four valence electrons and are connected to each other by a double bond. This must not be confused with the neutral Cd^0S^0 configuration, which is a mixed-bonding state. The expression for the static effective charge (see Coulson et al. 1962) is

$$\frac{e*}{e} = \frac{N(a/b)^2 - (8 - N)}{1 + (a/b)^2}, \tag{9}$$

with N as the valency. For $N = 2$, the effective charge vanishes when $a/b = \sqrt{3}$. For

Fig. 8 (**a**) Electronegativity
of the elements with groups
from the periodic table of
elements identified by
interconnecting lines.
(**b**) Ionicity of alkali halides
and halide molecules as a
function of the difference in
electronegativity (After
Pauling 1960)
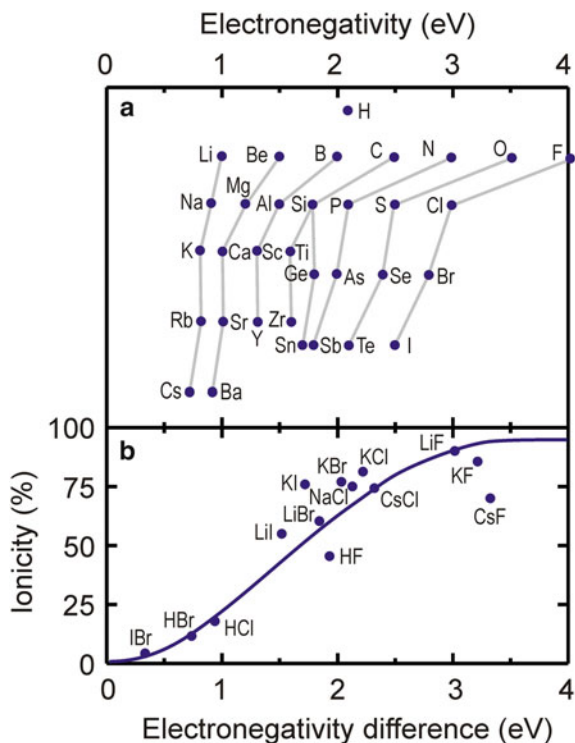
Table 4 Static effective charges of partially covalent *AB* compounds (After Coulson et al. 1962)

Compound	e^*/e	Compound	e^*/e
ZnO	0.60	BN	0.43
		AlN	0.56
		GaN	0.55
		InN	0.58
ZnS	0.47	BP	0.32
CdS	0.49	AlP	0.46
HgS	0.46	GaP	0.45
		InP	0.49
ZnSe	0.47	AlAs	0.47
CdSe	0.49	GaAs	0.46
HgSe	0.46	InAs	0.49
ZnTe	0.45	AlSb	0.44
CdTe	0.47	GaSb	0.43
HgTe	0.49	InSb	0.46

$N = 3$ in III–V compounds, e^* vanishes when $a/b = \sqrt{5/3}$, and for group IV
semiconductors when $a = b$.

In crystals, low coordination numbers (typically 4) signify a considerable cova-
lent contribution to the bonding.

Fig. 9 Schematic sketch of mixed bonding from (**a**) nearly perfect covalent in Ge to (**d**) perfect ionic in KCl. It shows diminishing bridge 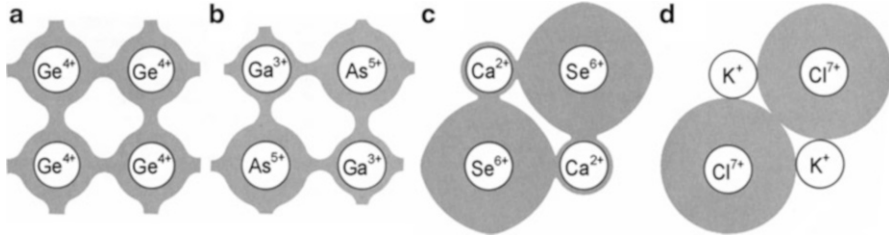formation and increasing cloud formation of electrons around anions with increasing ionicity (After Ashcroft and Mermin 1976)
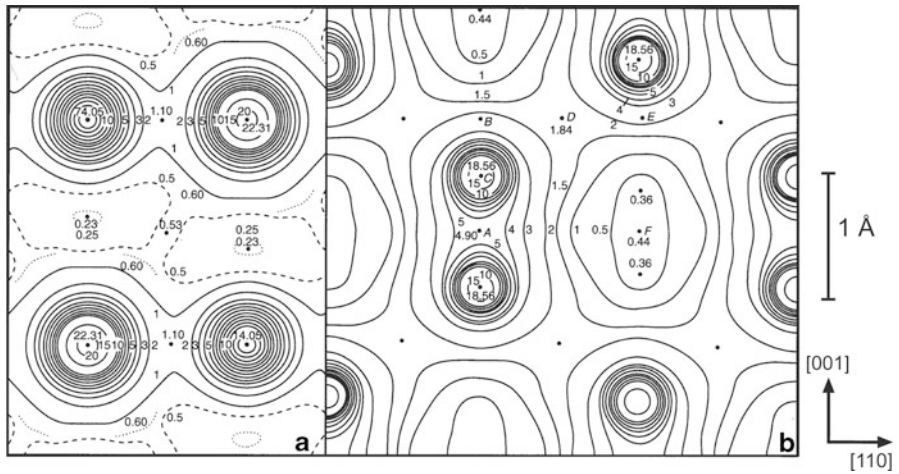
Fig. 10 Electron-density distribution obtained by Fourier analysis of the x-ray diffraction pattern of (**a**) NaCl, (110) plane, and (**b**) diamond, (110) plane (After Brill et al. 1939)

The different degree of bridge formation in crystals with mixed bonding (Fig. 9) can be made visible by a Fourier analysis of x-ray diffraction from which the electron-density distribution around each atom can be obtained. This is shown for a mostly ionic crystal in Fig. 10a and for a mostly covalent crystal in Fig. 10b.

2 Metallic Bonding

Metallic bonding can be understood as a collective interaction of a mobile electron fluid with metal ions. Metallic bonding occurs when the number of valence electrons is only a small fraction of the coordination number; then, neither an ionic nor a covalent bond can be established. Metallic bonding of simple metals, e.g., alkali metals, can be modeled by assuming that each metal atom has given up its valence electron, forming a lattice of positively charged ions, submerged in a fluid of

electrons. Between the repulsive electron–electron and ion–ion interactions and the attractive electron–ion interaction, a net attractive binding energy results, which is *nondirectional* and *not saturable*, and results in *close-packed structures* with high coordination numbers (8 or 12; Wigner and Seitz 1933), but relatively wide spacing between the submerged metal ions (Table 5). Such metals have low binding energies (~1 eV atom^{-1}) and high compressibility. They are mechanically soft, since the nondirectional lattice forces exert little resistance against plastic deformation. This makes metals attractive for forming and machining.

In other metals, such as transition-group elements, the bonding may be described as due to covalent bonds which rapidly hop from atom pair to atom pair. Again, free electrons are engaged in this resonance-type bonding. These metals have a higher binding energy of ~4 to 9 eV atom^{-1} and an interatomic distance that is closer to that given by the sum of ionic radii (Table 5). They are substantially harder when located in the middle of the transition metal row, e.g., Mo and W (Ashcroft and Mermin 1976).

In semiconductors with a very high density of free carriers, metallic binding forces may contribute a small fraction to the lattice bond, interfering with the predominant covalent bonding and usually weakening it, since these electrons are obtained by ionizing other bonds. Changes in the mechanical strength of the lattice can be observed in photoconductors in which a high density of free carriers can be created by light (Gorid'ko et al. 1961). For more information, see Ziman (1969) and Harrison (1966).

3   Further Types of Bonding in Solids

van der Waals Bonding Noble gas atoms or molecules with saturated covalent bonds can be bound to each other by dipole–dipole interaction (Debye). The dipole is created between the nucleus (nuclei) of the atom (molecule) and the cloud of electrons moving around these nuclei and forms a fluctuating dipole moment even for a spherically symmetrical atom. The interaction creates very weak, nonsaturable attractive forces. The weakness of this van der Waals interaction results in low melting points (Table 6) and soft *molecule crystals*. The bonding potential $V(r)$ is complemented by a short-range repulsive component originating from the Coulomb

Table 5 Ionic radii r_i and half the nearest-neighbor distances in metals r_m in Å (After Ashcroft and Mermin 1976)

Metal	r_i	r_m	r_m/r_i	Transition metal	r_i	r_m	r_m/r_i
Li	0.60	1.51	2.52	Cu	0.96	1.28	1.33
Na	0.95	1.83	1.93	Ag	1.26	1.45	1.15
K	1.33	2.26	1.70	Au	1.37	1.44	1.05
Rb	1.48	2.42	1.64				
Cs	1.69	2.62	1.55				

Table 6   Melting points (m.p.) of crystals bonded by van der Waals interaction

Noble gas crystal		Organic crystal		
Atom	m.p. (K)	Molecule	Formula	m.p. (°C)
He	0.95 (25 bar)	Anthracene	$C_{14}H_{10}$	216
Ne	25	Tetracene	$C_{18}H_{12}$	357
Ar	84	Pentacene	$C_{22}H_{14}$	300
Kr	116	Quaterthiophene	$C_{16}H_{10} S_4$	~213
Xe	162	Quinquethiophene	$C_{20}H_{12} S_5$	253
Rn	202	Hexathiophene	$C_{24}H_{14} S_6$	290
		Rubrene	$C_{42}H_{28}$	315–330

Fig. 11 Hydrogen bonding between a positive hydrogen ion (proton) and two ions (coordination number 2)
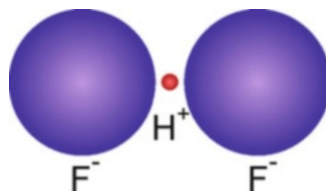
repulsion of the core electrons and nuclei; this component can be approximated by an exponential term, yielding, according to Buckingham (1938), the potential energy

$$eV = -\frac{A}{r^6} + B \ e^{-\alpha r} \tag{10}$$

with empirical parameters A, B, and α. van der Waals forces (van der Waals 1873) are the main binding forces of organic semiconductors (see Sect. 3.3).

Hydrogen Bonding   Hydrogen bonding (Fig. 11) is a type of ionic bonding in which the hydrogen atom has lost its electron to another atom of high electronegativity. The remaining proton establishes a strong Coulomb attraction. This force is not saturable. However, because of the small size of the proton, hydrogen bonding is strongly localized, and spatially no more than two ions have space to be attracted to it. When part of a molecule, the hydrogen bond – although ionic in nature – fixes the direction of the attached atom because of space consideration. It should not, however, be confused with the covalent bonding of hydrogen that occurs at dangling bonds (see ▶ Sect. 3.2.2 in chapter "The Structure of Semiconductors") in semiconductors, e.g., at the crystallite interfaces of polycrystalline Si or in amorphous Si:H.

Intermediate Valence Bonding   An interesting group of semiconductors are *transition-metal compounds*. The transition metals have partially filled *inner 3d*, *4d*, *5d*,

or $4f$ shells and a filled outer shell that provides a shielding effect to the valence electrons. In these compounds, the crystal field has a reduced effect. Some of these compounds show *intermediate valence bonding*. The resulting unusual properties range from resonant valence-exchange transport in copper oxide compounds (Anderson et al. 1987) to giant magnetoresistance and very large magneto-optical effects in rare-earth semiconductors. For a review, see Holtzberg et al. (1980).

Other Bonding Considerations Other, more subtle bonding considerations have gained a great deal of interest because of their attractive properties. These are related to magnetic and special dielectric properties, to superconductivity, as well as to other exotic effects.

For instance, diluted ("semi-") magnetic semiconductors such as the alloy $Cd_{1-x}Mn_xTe$ (Furdyna 1982, 1986; Brandt and Moshchalkov 1984; Wei and Zunger 1986; Goede and Heimbrodt 1988) show interesting magneto-optical properties. They change from paramagnetic ($x < 0.17$) to antiferromagnetic ($0.6 < x$) and to the ferro- or antiferromagnetic behavior of MnTe (▶ Sect. 2 in chapter "Magnetic Semiconductors"); they exhibit giant magneto-optical effects and bound magnetic polarons and offer opportunities for opto-electric devices that are tunable by magnetic fields.

These materials favor specific structures and permit the existence of certain quasiparticles, such as small polarons or Frenkel excitons. The discussion requires a substantial amount of understanding of the related physical effects and is therefore postponed to a more appropriate section of this book (see also Phillips 1973; Harrison 1980; Ehrenreich 1987).

3.1   Atomic and Ionic Radii

The equilibrium distances between atoms in a crystal define atomic radii when assuming hard-sphere atoms touching each other. In reality, however, these radii are soft with some variation of the electronic eigenfunctions and, for crystals with significant covalent fraction, with dependence on the angular atomic arrangement. However, for many crystals, the hard-sphere radii are very useful for most lattice estimates.

When comparing the lattice constants of chemically similar crystals, such as NaCl, NaBr, KCl, and KBr, one can determine the radii of the involved ions (Na^+, K^+, Cl^-, and Br^-) if at least one radius is known independently. Goldschmidt (1927) used the radii of F^- and 0^{--} for calibration. Consequently, listings of other ionic radii are therefore referred to as *Goldschmidt radii*. These radii are independent of the compound in which the atoms are incorporated as long as they exhibit the same type of bonding. One distinguishes atomic, ionic, metallic, and van der Waals radii. Ionic radii vary with changing valency.

A list of the most important ion and atomic radii is given in Table 7. The drastic change in radii with changing bonding force (Mooser and Pearson 1956) is best demonstrated by comparing a few typical examples for some typical elements

Table 7 Covalent (effective ionic charge $e^* = 0$) and standard ionic (identified by $\pm\, e^*$) radii in Å

e^*	+1	0		+2	0		+3	0		+4	0	−4		0	−3		0	−2
Li	0.68	1.34	Be	0.30	0.90	B	0.16	0.88	C		0.77	2.60	N	0.70	1.71	O	0.73	1.46
Na	0.98	1.54	Mg	0.65	1.30	Al	0.45	1.26	Si	0.38	1.17	2.71	P	1.10	2.12	S	1.04	1.90
K	1.33	1.96	Ca	0.94	1.74	Sc	0.68		Ti	0.60			As	1.18	2.22	Se	1.14	2.02
Cu	0.96		Zn	0.74	1.31	Ga	0.62	1.26	Ge	0.53	1.22	2.72						
Rb	1.48		Sr	1.10		Y	0.88		Zn	0.77			Sb	1.36	2.45	Te	1.32	2.22
Ag	1.26		Cd	0.97	1.48	In	0.81	1.44	Sn		1.40	2.94						
Cs	1.67		Ba	1.2		La	1.04		Ce	0.92			Bi	1.46		Po		2.30
Au	1.37		Hg	1.10	1.48	Tl	0.95	1.47	Pb	0.84	1.46						

incorporated in semiconductors (Fig. 12). For more recent estimates of tetrahedral covalent radii, see van Vechten and Phillips (1970).

The deviation from strict rigidity, i.e., the softness of the ionic spheres, is conventionally considered by using a softness parameter r_0 in the exponential repulsion formula (Eq. 2). This parameter is listed for a number of ions in Table 8.

This softness also results in a change of the standard ionic radii as a function of the number of surrounding atoms. A small correction Δ_m in the interionic distance is listed in Table 9. This needs to be considered when crystals with different coordination numbers m, i.e., the number of surrounding atoms, are compared with each other (e.g., CsCl and NaCl).

With increasing atomic number, the atomic (or ionic) radius of homologous elements increases. The cohesive force therefore decreases with increasing atomic (ionic) radii. Thus, compounds formed by the same bonding forces, and crystallizing with similar crystal structure, show a decrease, for example, in hardness,[5] melting point, and band gap, but an increase in dielectric constant and carrier mobility (see the respective sections).

The ratio of ionic radii determines the preferred crystal structure of *ionic* compounds. This is caused by the fact that the energy gain of a crystal is increased with every additional atom that can be added per unit volume. When several possible atomic configurations are considered, the material crystallizes in a modification that *maximizes* the number of atoms in a given volume. This represents the state of lowest potential energy of the crystal, which is the most stable one. An elemental crystal with isotropic radial interatomic forces will therefore crystallize in a close-packed structure. In a binary crystal, the ratio of atomic radii will influence the possible crystal structure. For isotropic nonsaturable interatomic forces, the resulting stable lattices are shown in Table 11 for different ratios of the ion radii (see following sections).

When a substantial amount of covalent bonding forces are involved, the rules to select a stable crystal lattice for a given compound are more complex. Here, atomic bond length and bond angles must be considered. Both can now be determined from basic principal density-functions calculations (see ▶ Sect. 2 in chapter "Quantum Mechanics of Electrons in Crystals"). We can then define atomic radii from the turning point of the electron-density distribution of each atom and obtain an angular-dependent internal energy scale from these calculations (Zunger and Cohen 1979). Using axes constructed from these radii, one obtains well-separated domains in which only one crystal structure is observed for binary compounds (Zunger and Cohen 1979; Villars and Calvert 1985; Yeh et al. 1992).

---

[5]This empirical quantity can be defined in several ways (e.g., as Mohs, Vickers, or Brinell *hardness*) and is a macroscopic mechanical representation of the cohesive strength of the lattice. In Table 10, the often used Mohs hardness is listed, which orders the listed minerals according to the ability of the higher-numbered one to scratch the lower-numbered minerals.

Fig. 12 Scale drawing of rigid sphere atoms with different bonding character [ionic or covalent, identified by the appropriate number of minus signs (*upper* row) or valence lines (*lower* row), respectively]
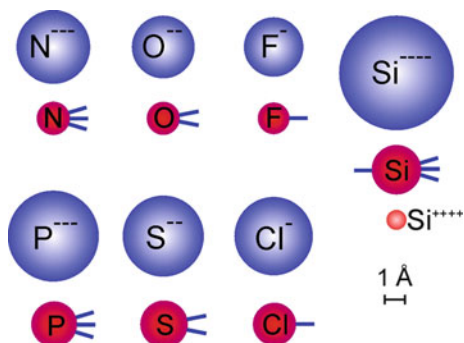

Table 8 Repulsion potential softness parameters (Eq. 2) in Å (After Shanker and Kumar 1987)

Ion	$r_0(th)$	$r_0(exp)$	Ion	$r_0(th)$	$r_0(exp)$
Li^-	0.069	0.042	F^-	0.179	0.215
Na^+	0.079	0.090	Cl^-	0.238	0.224
K^+	0.106	0.108	Br^-	0.258	0.254
Rb^+	0.115	0.089	I^-	0.289	0.315
Cs^+	0.130	0.100			

Table 9 Change of interatomic distance Δ_m (in Å) for compounds deviating from coordination number $m = 6$

m	Δ_m	m	Δ_m	m	Δ_m	Δ_m	Δ_m
1	−0.50	4	−0.11	7	+0.04	10	+0.14
2	−0.31	5	−0.05	8	+0.08	11	+0.17
3	−0.19	6	0	9	+0.11	12	+0.19

Table 10 Mohs hardness

Material	Chemistry	Lattice type	Hardness
Talc	$Mg_3H_2SiO_{12\text{-aq}}$	Layer lattice	1
Gypsum	$CaSO_4 \cdot H_2O$	Layer lattice	2
Iceland spar	$CaCO_3$	Layer lattice	3
Fluorite	CaF_2	Ion lattice	4
Apatite	$Ca_5F(PO_4)_3$	Ion lattice	5
Orthoclase	$KAlSi_3O_8$	SiO_4 frame	6
Quartz	SiO_2	SiO_4 frame	7
Topaz	$Al_2F_2SiO_4$	Mixed ion-valency lattice	8
Corundum	Al_2O_3	Valency lattice	9
Diamond	C	Valency lattice	10

Table 11 Preferred lattice structure for AB compounds with ionic binding forces (After Goldschmidt 1927)

r_A/r_B	Preferred stable lattice
<0.22	None
0.22…0.41	Zincblende or wurtzite
0.41…0.72	NaCl lattice
>0.72	CsCl lattice

Fig. 13 Variation of bond length in an $A_{1-x}B_xC$ alloy for rigid atoms ($\varepsilon = 1$), virtual crystal approximation ($\varepsilon = 0$), and experimentally observed relaxation
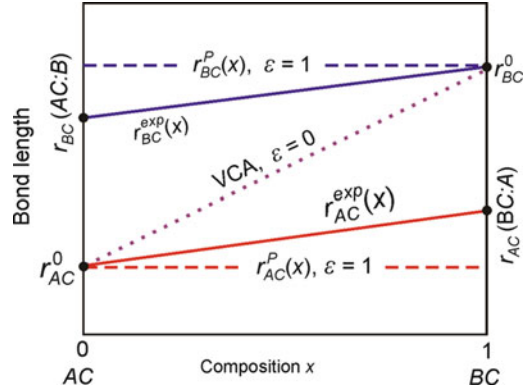
3.2 Bond-Length Relaxation in Alloys

The lattice constant of alloys $A_{1-x}B_xC$ of binary compounds AC and BC with respective lattice constants a_{AC} and a_{BC} interpolates according to the concentration

$$a(x) = (1 - x)a_{AC} + xa_{BC} \tag{11}$$

when they crystallize with the same crystal structure (Vegard's rule, Vegard 1921). However, the bond length between any of the three pairs of atoms is neither a constant, as suggested from the use of constant atomic radii (Pauling 1960), nor a linear interpolation as shown by the dotted line in Fig. 13 for total relaxation of the bond of atom B in a different chemical environment AC (or of A in BC).

This nonrigidity of atoms is important when incorporating isovalent impurities into the lattice of a semiconductor (doping) and estimating the resulting deformation of the surrounding lattice. With the bond length r_{BC} within the AC lattice (see Table 12), one defines a relaxation parameter

$$\varepsilon = \frac{r_{BC}(AC : B) - r_{AC}^0}{r_{BC}^0 - r_{AC}^0}. \tag{12}$$

The superscript 0 indicates the undisturbed pure crystal, the notation $AC{:}B$ indicates

B as doping element with a sufficiently small density incorporated in an AC compound, so that B–B interaction can be neglected.

The relaxation parameter can be estimated from the bond-stretching and bond-bending force constants α and β (see Table 13), according to Martins and Zunger (1984),

$$\varepsilon = \frac{1}{1 + \dfrac{1}{6}\dfrac{\alpha_{AC}}{\alpha_{BC}}\left(1 + 10\dfrac{\beta_{AC}}{\alpha_{AC}}\right)}, \tag{13}$$

yielding values of ε typically near 0.7 (see Table 12); that is, isovalent impurity

Table 12 Bond length of an isovalent impurity in a given host lattice and bond-length relaxation parameter (After Martins and Zunger 1984)

System	r_{BC} (AC:B) (Å)	ε	System	r_{BC} (AC:B) (Å)	ε
AlP:In	2.480	0.65	InP:Al	2.414	0.73
GaP:In	2.474	0.63	InP:Ga	2.409	0.73
AlAs:In	2.553	0.60	InAs:Al	2.495	0.74
GaAs:In	2.556	0.62	InAs:Ga	2.495	0.73
AlSb:In	2.746	0.61	InSb:Al	2.693	0.75
GaSb:In	2.739	0.60	InSb:Ga	2.683	0.74
AlP:As	2.422	0.65	AlAs:P	2.395	0.67
AlP:Sb	2.542	0.61	AlSb:P	2.444	0.73
AlAs:Sb	2.574	0.60	AlSb:As	2.510	0.71
GaP:As	2.414	0.62	GaAs:P	2.387	0.68
GaP:Sb	2.519	0.57	GaSb:P	2.436	0.73
GaAs:Sb	2.564	0.60	GaSb:As	2.505	0.70
InP:As	2.595	0.67	InAs:P	2.562	0.74
InP:Sb	2.700	0.60	InSb:P	2.597	0.79
InAs:Sb	2.739	0.64	InSb:As	2.667	0.75
ZnS:Se	2.420	0.70	ZnSe:S	2.367	0.78
ZnS:Te	2.539	0.67	ZnTe:S	2.407	0.78
ZnSe:Te	2.584	0.71	ZnTe:Se	2.502	0.74
β-HgS:Se	2.611	0.76	HgSe:S	2.553	0.80
β-HgS:Te	2.716	0.71	HgTe:S	2.579	0.82
HgSe:Te	2.748	0.74	HgTe:Se	2.665	0.80
ZnS:Hg	2.482	0.73	β-HgS:Zn	2.380	0.80
ZnSe:Hg	2.587	0.74	HgSe:Zn	2.494	0.78
ZnTe:Cd	2.755	0.70	CdTe:Zn	2.674	0.78
ZnTe:Hg	2.748	0.69	HgTe:Zn	2.673	0.78
γ-CuCl:Br	2.440	0.81	γ-CuBr:Cl	2.367	0.79
γ-CuCl:I	2.563	0.80	γ-CuI:Cl	2.407	0.76
γ-CuBr:I	2.585	0.79	γ-CuI:Br	2.500	0.76
C:Si	1.665	0.35	Si:C	2.009	0.74
Si:Ge	2.380	0.58	Ge:Si	2.419	0.63
Si:Sn	2.473	0.53	α-Sn:Si	2.645	0.70
Ge:Sn	2.549	0.55	α-Sn:Si	2.688	0.67

Table 13 Bond-length (d), bond-stretching (α), and bond-bending (β) force constants, calculated from elastic constants (After Martin 1970)

Crystal	d (Å)	α (N m^{-1})	β (N m^{-1})	Crystal	d (Å)	α (N m^{-1})	β (N m^{-1})
C	1.545	129.33	84.71	InP	2.541	43.04	6.24
Si	2.352	48.50	13.82	InAs	2.622	35.18	5.49
Ge	2.450	38.67	11.37	InSb	2.805	26.61	4.28
α-Sn	2.810	25.45	6.44	ZnS	2.342	44.92	4.81
SiC	1.888	88.	47.5	ZnSe	2.454	35.24	4.23
AlP	2.367	47.29	9.08	ZnTe	2.637	31.35	4.45
AlAs	2.451	43.05	9.86	CdTe	2.806	29.02	2.44
AlSb	2.656	35.35	6.79	β-HgS	2.534	41.33	2.56
GaP	2.360	47.32	10.46	HgSe	2.634	36.35	2.36
GaAs	2.448	41.19	8.94	HgTe	2.798	27.95	2.57
GaSb	2.640	33.16	7.23	γ-CuCl	2.341	22.9	1.01
				γ-CuBr	2.464	23.1	1.32
				γ-CuI	2.617	22.5	2.05

atoms behave more like rigid atoms ($\varepsilon = 1$) than totally relaxed atoms ($\varepsilon = 0$) in a virtual crystal approximation (Eq. 11).

3.3 Bonding in Organic Crystals

Recently, semiconductors made from organic materials gained much advertence[6]; for a review, see Schwoerer and Wolf (2007). All organic semiconductors are solids comprising molecules with carbon atoms, which are bond by a system of *conjugated π electrons*. In such a system, two adjacent C atoms are not only bond by σ bonds (see Fig. 3), i.e., single bonds, but in addition by multiple (usually double) bonds. A simple example is the ethene molecule C_2H_4 illustrated in Fig. 14. Three of the four valence electrons ($2s^2$, $2p^2$) of each C atom form σ bonds from sp^2 hybrid orbitals: two to H atoms and one to the other C atom; all these bonds lie in one plane. The two remaining p_z electrons of the C atoms have their density distribution above and below this plane; they form an additional π bond, which is weaker than the strong σ bond because the overlap of the p_z wave functions of the adjacent C atoms is small.

The larger molecules of organic semiconductors have delocalized conjugated π electrons in alternating single and double bonds. The molecule may be linear or cyclic as illustrated in Fig. 15.

The molecules are the building blocks of organic semiconductors. They may either be arranged in a regular order of a crystal as shown in ▶ Sect. 1.5 in chapter

---

[6]Two principal devices made of organic semiconductors recently entered the market: light-emitting diodes (OLEDs) and field-effect transistors (OFETs), processed as thin-film transistors (TFT). Prominent molecules used in organic (opto-) electronics are listed in ▶ Sect. 1.5 in chapter "The Structure of Semiconductors."

Fig. 14 σ (*blue*) and π
(*green*) molecule orbitals of
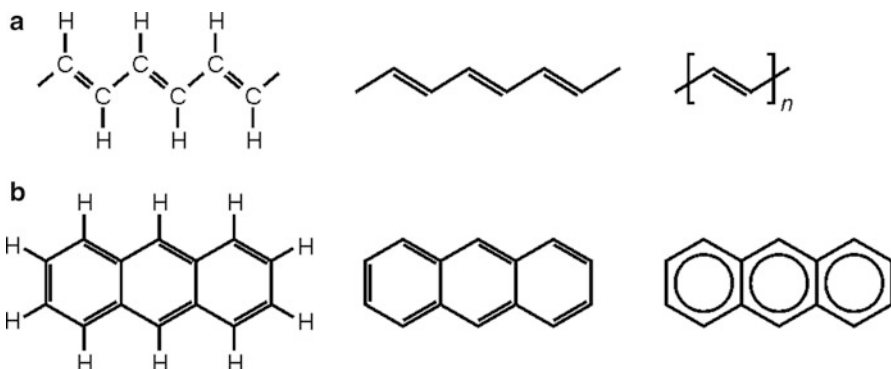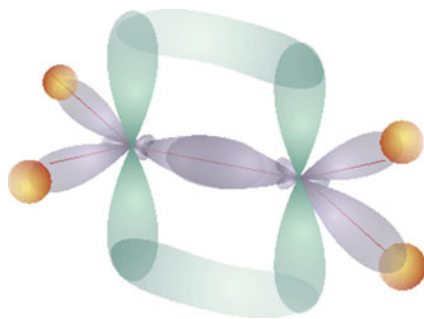an ethene molecule C_2H_4

Fig. 15 Various representations of (**a**) polyethylene and (**b**) anthracene. Carbon atoms are generally left out and usually also the hydrogen atoms. The π electrons are indicated by double valence lines or, in cyclic molecules, also by a circle

"The Structure of Semiconductors" or irregularly; while both forms are applied for organic electronics, generally best performance is obtained with crystalline modifications. The molecules of organic semiconductors do not have unsaturated bonds and hence no free valences like the atoms of inorganic semiconductors. Intermolecular bonding forces of electrically neutral and nonpolar molecules are pure van der Waals interactions. If the molecules have a permanent dipole moment or polar substituents, static dipolar bonding and ionic or hydrogen bonding may be superimposed. In the presence of charges, a term $+ q_1 q_2/r$ is added to the potential in Eq. 10 (see Starr and Williams 1977).

The bonding energy provided by van der Waals interaction is expressed by Eq. 10. However, in contrast to interatomic distances in noble gas crystals, the distance r in Eq. 10 is not well defined in organic solids: the distance between the molecules is of the same size as the extension of the molecules. A good description of experimental data is obtained, if the attractive potential between two neighboring molecules is calculated as the sum of all atom – atom potentials according to the Buckingham potential (Eq. 10), where r is the distance from an atom of one molecule to an atom of the other molecule (Kitaigorodskii 1966). Parameters of Eq. 10 for all

Table 14 Parameters of the Buckingham potential Eq. 10 for atom – atom pairs of neighboring hydrocarbon molecules (After Starr and Williams 1977)

Pair	A (kJ mol^{-1} Å^6)	B (kJ mol^{-1})	α (Å^{-1})
C–C	2,140	300,000	3.60
C–H	467	35,600	3.67
H–H	102	9,080	3.74

Fig. 16 Intermolecular potential of Eq. 10 for different atom – atom pairs of neighboring hydrocarbon molecules. The *curves* were computed using the parameters of Table 14
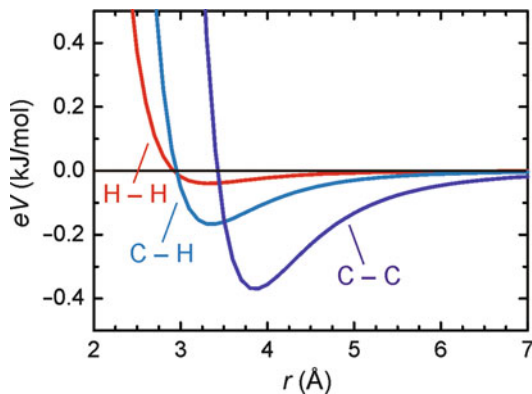
three different pairs of atoms occurring in hydrocarbon molecules are listed in Table 14. The parameters were deduced from structural data and heat of sublimation of many organic molecules and apply in good approximation for all solids composed of hydrocarbon molecules with conjugated π electrons. The intermolecular atom – atom potential calculated with these parameters is shown in Fig. 16. The intermolecular bond lengths and energies per atom pair are 3.88 Å, 4.1 meV for C–C; 3.30 Å, 2.1 meV for C–H; and 3.37 Å, 0.4 meV for H–H.

4 Summary

The interatomic forces responsible for crystal bonding are, to a large degree, electrostatic forces between the electrons and atomic nuclei. These Coulomb forces are the basic element for ionic and hydrogen bonding forces but are also involved in metallic bonding and, as dipole–dipole interaction, in van der Waals bonding. In addition, strong quantum-mechanical effects, determining specific orbitals, and Pauli exclusion are major contributing factors in covalent and metallic bonding, respectively. While the overlap of eigenfunctions of unpaired electrons with opposite spin provides the major contribution to the covalent attraction, the near impermeability of all other electronic orbitals determines the rigidity of atoms in close proximity to each other. This justifies the specification of atomic radii.

References

Anderson PW, Baskaran G, Zou Z, Hsu T (1987) Resonating–valence-bond theory of phase transitions and superconductivity in La_2CuO_4-based compounds. Phys Rev Lett 58:2790

Ashcroft NW, Mermin ND (1976) Solid state physics. Holt Reinhart and Winston, New York

Born M (1919) Die Elektronenaffinität der Halogenatome. Verh Dtsch Phys Ges 21:679 (The electron affinity of halogen atoms, in German)

Born M, Huang K (1954) Dynamical theory of crystal lattices. Oxford University Press, London

Born M, Landé A (1918) Über die Berechnung der Kompressibilität regulärer Kristalle aus der Gittertheorie. Verh Dtsch Phys Ges 20:210 (On computing the compressibility of normal crystals applying lattice theory, in German)

Brandt NB, Moshchalkov VV (1984) Semimagnetic semiconductors. Adv Phys 33:193

Brill R, Grimm HG, Hermann C, Peters CL (1939) Anwendung der röntgenographischen Fourieranalyse auf Fragen der chemischen, Bindung. Ann Physik, Lpz 34:26 (Application of x-ray Fourier analysis to problems of the chemical bond, in German)

Buckingham RA (1938) The classical equation of state of gaseous Helium, Neon and Argon. Proc R Soc Lond Ser A Math Phys Sci 168:264–283

Cotton FA, Wilkinson G (1972) Advanced inorganic chemistry: a comprehensive text, 3rd edn. Interscience, New York

Coulson CA, Redei LB, Stocker D (1962) The electronic properties of tetrahedral intermetallic compounds. I. Charge distribution. Proc R Soc Lond A 270:357

Dawson B (1967) A general structure factor formalism for interpreting accurate x-ray and neutron diffraction data. Proc Roy Soc Lond A 298:255

Ehrenreich H (1987) Electronic theory for materials science. Science 235:1029

Furdyna JK (1982) Diluted magnetic semiconductors: an interface of semiconductor physics and magnetism. J Appl Phys 53:7637

Furdyna JK (1986) Diluted magnetic semiconductors: issues and opportunities. J Vac Sci Technol A 4:2002

Goede O, Heimbrodt W (1988) Optical Properties of (Zn, Mn) and (Cd, Mn) chalcogenide mixed crystals and superlattices. Phys Stat Sol B 146:11

Goldschmidt VM (1927) Geochemische Verteilungsgesetze der Elemente, Skrifter det Norske Videnskaps. Akad (Oslo), I Math Naturwiss Kl 1926:7 (Laws for the geometrical distribution of the elements, in German)

Gorid'ko NY, Kuzmenko PP, Novikov NN (1961) Change in mechanical properties of germanium caused by the change of concentration of current carriers. Fiz Tverd Tela 3:3650

Haber F (1919) Theory of the heat of reaction. Verh Dtsch Phys Ges 21:750

Harrison WA (1966) Pseudopotentials in the theory of metals. W.A. Benjamin, New York

Harrison WA (1980) Electronic structure and the properties of solids: the physics of chemical bonds. Freeman, San Francisco

Holtzberg F, von Molnar S, Coey JMD (1980) Rare earth magnetic semiconductors. In: Moss TS, Keller SP (eds) Handbook of semiconductors, Vol. 3: materials properties and preparation. North Holland, Amsterdam

Kitaigorodskii AI (1966) Stacking of molecules in a crystal, interaction potential between atoms not linked by valence bonds, and calculation of molecular movements. J Chim Phys 63:9

Kittel C (1996) Introduction to solid state physics, 7th edn. Wiley, New York

Madelung E (1918) Das elektrische Feld in Systemen von regelmässig angeordneten Punktladungen. Phys Z 19:524 (The electric field of systems of regularly arranged point charges, in German)

Martin RM (1970) Elastic properties of ZnS structure semiconductors. Phys Rev B 1:4005

Martins JL, Zunger A (1984) Bond lengths around isovalent impurities and in semiconductor solid solutions. Phys Rev B 30:6217

Mooser E, Pearson WB (1956) The chemical bond in semiconductors. J Electron 1:629

Pauling L (1960) The nature of the chemical bond. Cornell University Press, Ithaca

Phillips JC (1973) Bonds and bands in semiconductors. Academic Press, New York

Schwoerer M, Wolf HC (2007) Organic molecular solids. Wiley-VCH, Weinheim

Shanker J, Kumar M (1987) Ion-dependent and crystal-independent interionic potentials. Phys Stat Sol B 142:325

Sherman J (1932) Crystal energies of ionic compounds and thermochemical applications. Chem Rev 11:93

Starr TL, Williams DE (1977) Coulombic nonbonded interatomic potential functions derived from crystal-lattice vibrational frequencies in hydrocarbons. Acta Cryst A 33:771

van der Waals JD (1873) Over de Continuiteit van den gasen vloeistoftoestand. Sijthoff, Leiden (On the continuity of the gaseous and liquid state, in Dutch)

van Vechten JA, Phillips JC (1970) New set of tetrahedral covalent radii. Phys Rev B 2:2160

Vegard L (1921) Die Konstitution der Mischkristalle und die Raumfüllung der Atome. Z Phys 5:17 (The configuration of mixed crystals and space filling of atoms, in German)

Villars P, Calvert LD (1985) Pearson's handbook of crystallographic data for intermetallic phases. American Society for Metals, Metals Park

Wei S-H, Zunger A (1986) Total-energy and band-structure calculations for the semimagnetic $Cd_{1-x}Mn_xTe$ semiconductor alloy and its binary constituents. Phys Rev B 35:2340

Weißmantel C, Hamann C (1979) Grundlagen der Festkörperphysik. Springer, Berlin (Fundamentals of solid state physics, in German)

Welker H, Weiss H (1954) Zur transversalen magnetischen Widerstandsänderung von InSb. Z Phys 138:322 (On the change of the transversal magnetic resistance on InSb, in German)

Wigner EP, Seitz F (1933) On the constitution of metallic sodium. Phys Rev 43:804

Yeh C-Y, Lu ZW, Froyen S, Zunger A (1992) Zinc-blende–wurtzite polytypism in semiconductors. Phys Rev B 46:10086

Ziman JM (1969) The physics of metals, Vol. 1, electrons. Cambridge University Press, London

Zunger A, Cohen ML (1979) First-principles nonlocal-pseudopotential approach in the density-functional formalism. II. Application to electronic and structural properties of solids. Phys Rev B 20:4082